

Probing Higgs portals with matrix-element based kinematic discriminants in $ZZ \rightarrow 4\ell$ production

Ulrich Haisch¹ and Gabriël Koole¹

¹*Max Planck Institute for Physics, Föhringer Ring 6, 80805 München, Germany*

E-mail: haisch@mpp.mpg.de, koole@mpp.mpg.de

ABSTRACT: A Higgs portal in the form of the operator $|H|^2$ provides a minimal and theoretically motivated link between the Standard Model (SM) and new physics. While Higgs portals can be constrained well by exotic Higgs decays if the beyond-the-SM states are light, testing scenarios where these particles are kinematically inaccessible is known to be challenging. We explore the sensitivity of future hadron collider measurements of $ZZ \rightarrow 4\ell$ production in constraining Higgs portal interactions. It is shown that by using a matrix-element based kinematic discriminant the reach of the high-luminosity option of the Large Hadron Collider (LHC) can be significantly enhanced compared to studies that are based on measurements of the four-lepton invariant mass spectrum alone. We also analyse the potential of the high-energy upgrade of the LHC and a Future Circular Collider in constraining new physics that couples to $|H|^2$. The obtained constraints are compared to the limits one expects to find from other single-Higgs probes. In addition, we provide an independent analysis of the relevant Higgs portal effects in double-Higgs production. We find that the constraints obtained from our $ZZ \rightarrow 4\ell$ analysis turn out to be both competitive with and complementary to the projected limits obtained using other search techniques.

Contents

1	Introduction	1
2	Higgs portal effects in $gg \rightarrow h^* \rightarrow ZZ$	3
3	ME-based kinematic discriminant	4
4	HL-LHC analysis	6
5	HE-LHC and FCC analyses	10
6	Discussion and outlook	11
A	Systematic uncertainties	15
B	Details of the double-Higgs calculation	15

1 Introduction

The discovery of a new spin-0 state by ATLAS and CMS [1, 2] with approximately the properties of the Standard Model (SM) Higgs boson has opened up new avenues in the pursuit of physics beyond the SM (BSM). In fact, there are both experimental and theoretical arguments that suggest that the Higgs boson may provide a window into BSM physics. Experimentally, the Higgs sector is far less explored and constrained compared to the gauge or fermionic sector of the SM [3, 4], while theoretically the SM Higgs doublet H plays a special role because it allows to write down relevant and marginal operators of the form $|H|^2\mathcal{O}$ with \mathcal{O} itself a gauge-invariant operator with a mass dimension of two or lower.

The simplest and most studied case of such an operator is $\mathcal{O} = \phi^2$ where ϕ is a real scalar that is a singlet under the SM gauge group but odd under a \mathbb{Z}_2 symmetry [5–9]. The corresponding interaction Lagrangian reads

$$\mathcal{L}_{H\phi} = -c_\phi |H|^2 \phi^2. \tag{1.1}$$

Notice that the \mathbb{Z}_2 symmetry acts on the real scalar field as $\phi \rightarrow -\phi$, which guarantees the stability of ϕ making it a suitable dark matter (DM) candidate. See for instance [10–12] for recent reviews of the ensuing DM phenomenology. In particular, under the assumption that ϕ is a relic of standard thermal freeze-out production DM direct detection experiments are known to foster stringent constraints on DM portals of the form (1.1) — see for example [12] and references therein. In theories with a non-thermal cosmological history, a real scalar ϕ can however be shown to be a viable DM candidate for a wide range of Higgs portal

realisations while evading existing experimental limits [13]. This opens up the possibility to probe (1.1) at high-energy colliders.

Another motivation for the existence of sizeable Higgs portal couplings to $|H|^2$ is provided by the hierarchy problem of the Higgs-boson mass. In fact, in models where the hierarchy problem is addressed by the addition of N_r real scalar top partners ϕ_i the relevant interaction Lagrangian can be written as [14]

$$\mathcal{L}_{H\phi_i} = -\frac{2N_c}{N_r} y_t^2 |H|^2 \sum_{i=1}^{N_r} \phi_i^2, \quad (1.2)$$

where $N_c = 3$ is the number of colours in QCD and $y_t = \sqrt{2}m_t/v \simeq 0.94$ is the top-quark Yukawa coupling with $m_t \simeq 163$ GeV the top-quark $\overline{\text{MS}}$ mass and $v \simeq 246$ GeV the Higgs vacuum expectation value. Well-known cases where (1.2) is a proxy for the resulting Higgs portal interactions are stops in the minimal supersymmetric SM (MSSM) and singlet scalar top partners in the hyperbolic Higgs [15] or tripled top model [16], if one assumes that these particles are approximately degenerate in mass. Notice that in such a case the interactions (1.1) and (1.2) are equivalent from the perspective of collider phenomenology if $|c_\phi| = 2N_c/\sqrt{N_r}y_t^2$. In the case of the MSSM, the hyperbolic Higgs and the tripled top model where $N_r = 12$, a light Higgs boson is therefore natural if one effectively has a Higgs portal of the form (1.1) with coupling strength $|c_\phi| \leq \sqrt{3}y_t^2 \simeq 1.5$.

The level of difficulty to discover or to exclude Higgs portals of the form (1.1) and (1.2) at high-energy colliders depends mainly on the mass m_ϕ of the new states that couple to $|H|^2$. While in the case of $m_\phi < m_h/2 \simeq 62.5$ GeV the decays of the Higgs boson into invisible [17–21] or undetected [4, 12] final states provide stringent constraints on the effective coupling strength of the Higgs portals, obtaining relevant constraints above the kinematic threshold $m_\phi > m_h/2$ turns out to be significantly more challenging. In fact, only two categories of collider measurements are known that provide sensitivity to Higgs portals above the kinematic threshold: firstly, pair-production of the new scalars in off-shell Higgs processes such as the vector-boson fusion (VBF), the $t\bar{t}h$ and the gluon-gluon-fusion (ggF) channel [22–36], and secondly, studies of the virtual effects that these particles produce when exchanged in loop diagrams that contribute to processes such as associated Zh , double-Higgs and $gg \rightarrow h^* \rightarrow ZZ$ production [37–43]. The existing analyses have considered a wide range of future high-energy hadron as well as lepton colliders, including the high-luminosity (HL) and high-energy (HE) versions of the Large Hadron Collider (LHC), a Future Circular Collider (FCC), the International Linear Collider (ILC), the Compact Linear Collider (CLIC) and a muon collider.

In this article, we investigate the sensitivity of future hadron collider measurements of off-shell Higgs production in the $pp \rightarrow ZZ \rightarrow 4\ell$ channel to Higgs portal interactions such as (1.1) and (1.2). Compared to earlier studies [34, 41, 42, 44] that relied on the four-lepton invariant mass ($m_{4\ell}$) spectrum alone to separate signal from background, we instead employ a matrix-element (ME) based kinematic discriminant in our work. Being sensitive not only to $m_{4\ell}$ but also to another seven variables such as the invariant masses of the two opposite-sign lepton pairs (for details consult the articles [45–48]), ME-based discriminants

fully exploit the event kinematics. As in our recent study [49], we find that the use of a ME method leads to a significantly improved coverage of the BSM parameter space, i.e. c_ϕ and m_ϕ in the case of (1.1), than a shape analysis of the $m_{4\ell}$ distribution. Motivated by this finding, we analyse in detail the HL-LHC, HE-LHC and FCC potential of the proposed method in constraining BSM physics that couples to the operator $|H|^2$.

Our work is structured as follows. In Section 2 we briefly discuss the calculation of the loop corrections to $pp \rightarrow ZZ \rightarrow 4\ell$ production arising from (1.1). The aforementioned ME-based kinematic discriminant is introduced in Section 3 where we also discuss how higher-order QCD corrections are taken into account in our study. The numerical analysis of the HL-LHC reach is performed in Section 4 and contains a comparison between the sensitivities obtained from a shape analysis of the $m_{4\ell}$ spectrum and the proposed ME method. In Section 5 we present our HE-LHC and FCC projections. We discuss our main results in Section 6, comparing them to the limits one expects to obtain from other single- and double-Higgs probes, and provide a short outlook. A discussion of the impact that different assumptions on the systematic uncertainties in our ME-based search strategy have on the projected constraints is relegated to Appendix A, while further details of the relevant loop calculations and their implementation in the Monte Carlo (MC) code for our double-Higgs analysis are given in Appendix B.

2 Higgs portal effects in $gg \rightarrow h^* \rightarrow ZZ$

At the one-loop level the $gg \rightarrow h^* \rightarrow ZZ$ process receives contributions from Feynman graphs such as the one displayed in Figure 1 that contains a modified Higgs propagator with insertions of the Higgs portal operator (1.1). The corresponding renormalised contribution to the self-energy of the Higgs takes the form

$$\hat{\Sigma}(\hat{s}) = \Sigma(\hat{s}) + (\hat{s} - m_h^2) \delta Z_h - \delta m_h^2, \quad (2.1)$$

where the bare Higgs self-energy, the one-loop corrections to the Higgs wave function and the mass counterterm in the on-shell scheme are given by the following expressions

$$\begin{aligned} \Sigma(\hat{s}) &= \frac{1}{(4\pi)^2} \left[c_\phi A_0(m_\phi^2) + 2v^2 |c_\phi|^2 B_0(\hat{s}, m_\phi^2, m_\phi^2) \right], \\ \delta Z_h &= -\frac{2v^2 |c_\phi|^2}{(4\pi)^2} \frac{d}{d\hat{s}} B_0(\hat{s}, m_\phi^2, m_\phi^2) \Big|_{\hat{s}=m_h^2}, \\ \delta m_h^2 &= \frac{1}{(4\pi)^2} \left[c_\phi A_0(m_\phi^2) + 2v^2 |c_\phi|^2 B_0(m_h^2, m_\phi^2, m_\phi^2) \right]. \end{aligned} \quad (2.2)$$

Here $\hat{s} = p^2$ with p the external four-momentum entering the Higgs propagator and the A_0 and B_0 functions are one- and two-point Passarino-Veltman scalar integrals defined as in [50, 51]. The expression in (2.2) can be easily generalised to other Higgs portals of the form (1.1). For instance, in the case of $\mathcal{L}_{H\Phi} = -c_\Phi |H|^2 |\Phi|^2$ with Φ a complex scalar field one just has to make the substitutions $c_\phi \rightarrow c_\Phi/\sqrt{2}$ and $m_\phi \rightarrow m_\Phi$.

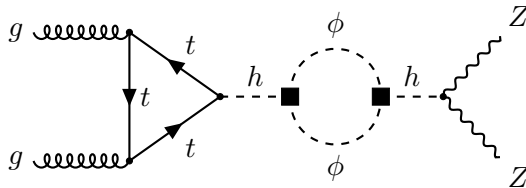


Figure 1: Example of a one-loop correction to $gg \rightarrow h^* \rightarrow ZZ$ production with insertions of the Higgs portal operator (1.1) indicated by the black boxes. Also diagrams with tadpoles or counterterms contribute but are not shown explicitly. Consult the main text for further details.

Notice that the contribution to the Higgs wave-function renormalisation constant δZ_h coming from the propagator corrections exactly cancels against those of the vertices when combined to obtain the full BSM contribution to the off-shell $gg \rightarrow h^* \rightarrow ZZ$ amplitude. Similarly, the tadpole contribution proportional to $A_0(m_\phi^2)$ also cancels in the difference $\Sigma(\hat{s}) - \delta m_h^2$. In contrast, the Higgs wave-function renormalisation constant δZ_h does not drop out in the on-shell Higgs signal strengths μ_i^f for production in channel i and decay in channel f . In terms of the inclusive Higgs production cross sections σ_i and the Higgs branching ratios BR_f , these quantities take the form

$$\mu_i^f = \frac{\sigma_i}{\sigma_i^{\text{SM}}} \frac{\text{BR}_f}{\text{BR}_f^{\text{SM}}} = 1 + \delta Z_h, \quad (2.3)$$

i.e. they receive a universal correction proportional to the Higgs wave-function renormalisation constant as given in (2.2). This feature allows to set indirect constraints on Higgs portal models by precision measurements of Higgs properties [38], which will be discussed in Section 6.

3 ME-based kinematic discriminant

The Higgs propagator corrections (2.1) and the relevant vertex counterterms have been implemented into version 8.0 of the event generator MCFM [52] to obtain kinematic distributions for $pp \rightarrow ZZ \rightarrow 4\ell$ such as the $m_{4\ell}$ spectrum. In addition, our MC code is also able to calculate the following ME-based kinematic discriminant [53–55]

$$D_S = \log_{10} \left(\frac{P_h}{P_{gg} + c \cdot P_{q\bar{q}}} \right). \quad (3.1)$$

Here P_h denotes the squared ME for the $gg \rightarrow h^* \rightarrow ZZ \rightarrow 4\ell$ process, P_{gg} is the squared ME for all gg -initiated channels (including the Higgs channel, the continuum background and their interference) and $P_{q\bar{q}}$ is the squared ME for the $q\bar{q} \rightarrow ZZ \rightarrow 4\ell$ process. Like in [53–55] the constant c is set to 0.1 to balance the $q\bar{q}$ - and gg -initiated contributions. We stress that in the SM more than 99% of the $pp \rightarrow ZZ \rightarrow 4\ell$ cross section falls into

the range of $-4.5 < D_S < 0.5$ [53]. For BSM models that predict events with $D_S < -4.5$ or $D_S > 0.5$ the variable D_S therefore presents a null test.

Currently, calculations of higher-order QCD corrections to four-lepton production via $q\bar{q}$ annihilation include the full next-to-next-to-leading order (NNLO) corrections and top-quark mass effects [56–59]. Next-to-leading order (NLO) corrections to the loop-induced gg channel have been computed by now as well [61–64], while for inclusive Higgs production the precision has been pushed to the next-to-next-to-next-to-leading order (N³LO) in the heavy top-quark limit [65]. As the $gg \rightarrow ZZ$ process starts contributing only at $\mathcal{O}(\alpha_s^2)$, it is part of the NNLO QCD corrections to ZZ production and NLO corrections to this channel formally contribute at N³LO. Lastly, NLO electroweak (EW) corrections could in principle play an important role as well. Within the SM they were combined with NNLO QCD effects for ZZ production in the work [66]. However, it has been shown in the paper [67] that including NLO EW effects in the SM has only a very minor effect on the sensitivity of indirect single-Higgs analyses to modifications of the trilinear Higgs coupling. We expect a similar pattern to arise in the context of the Higgs portal models studied here. A dedicated simulation of four-lepton events including both higher-order QCD as well as EW corrections both in and beyond the SM, consistently matched to a parton shower and including detector effects is clearly beyond the scope of the present article and therefore left for future work.

In order to include higher-order QCD corrections in our $pp \rightarrow ZZ \rightarrow 4\ell$ analysis, we proceed as in our recent publication [49]. For the two relevant production channels we calculate the so-called K -factor defined as the ratio between the fiducial cross section at a given order in QCD and the corresponding leading order (LO) QCD prediction. In the case of the gg -initiated contribution we utilise the results of [60]. The ratio between the NLO and LO ggF predictions turns out to be essentially flat in $m_{4\ell}$ and by averaging we find $K_{gg}^{\text{NLO}} = 1.83$. This number agrees with the K -factors reported in [61, 63, 64]. In the case of the $q\bar{q}$ -initiated contribution we use the NNLO results obtained in [63]. The relevant K -factor again turns out to be basically flat in $m_{4\ell}$ with a central value of $K_{q\bar{q}}^{\text{NNLO}} = 1.55$. This finding is in accordance with [56]. The quoted K -factors are then used to obtain a QCD-improved prediction for the $pp \rightarrow ZZ \rightarrow 4\ell$ cross section differential in the variable O as follows:

$$\frac{d\sigma_{pp}}{dO} = K_{gg}^{\text{NLO}} \left(\frac{d\sigma_{gg}}{dO} \right)_{\text{LO}} + K_{q\bar{q}}^{\text{NNLO}} \left(\frac{d\sigma_{q\bar{q}}}{dO} \right)_{\text{LO}} . \quad (3.2)$$

Notice that (3.2) is accurate in the case of the $m_{4\ell}$ spectrum. For the D_S distribution one observes [49] a close to flat K -factor of around 1.6 between the LO and the improved prediction (3.2). It is furthermore found that the inclusion of higher-order QCD corrections reduces the scale uncertainties by a factor of about 3 from (7–8)% to (2–3)%. The fact that the central value of the improved D_S spectrum lies outside the LO uncertainty bands demonstrates that the scale variations of (3.2) do not provide a reliable way to estimate the size of higher-order QCD effects. In view of this and given that the discriminant D_S as defined in (3.1) is only LO accurate, we will make different assumptions on the systematic uncertainties entering our ME-based search strategy, a point we will discuss in more detail in our numerical analyses presented in Sections 4 and 5 as well as

in Appendix A. A similar approach is also used in the projections [68, 69] that estimate the HL-LHC reach in constraining off-shell Higgs boson production and the Higgs boson total width in $pp \rightarrow ZZ \rightarrow 4\ell$.

4 HL-LHC analysis

In our $pp \rightarrow ZZ \rightarrow 4\ell$ analysis we consider the window $140 \text{ GeV} < m_{4\ell} < 600 \text{ GeV}$ of four-lepton invariant masses. The charged leptons are required to be in the pseudorapidity range $|\eta_\ell| < 2.5$ and the lepton with the highest transverse momentum (p_T) must satisfy $p_{T,\ell_1} > 20 \text{ GeV}$ while the second, third and fourth lepton in p_T order is required to obey $p_{T,\ell_2} > 15 \text{ GeV}$, $p_{T,\ell_3} > 10 \text{ GeV}$ and $p_{T,\ell_4} > 6 \text{ GeV}$, respectively. The lepton pair with the mass closest to the Z -boson mass is referred to as the leading dilepton pair and its invariant mass is required to be within $50 \text{ GeV} < m_{12} < 106 \text{ GeV}$, while the subleading lepton pair must be in the range of $50 \text{ GeV} < m_{34} < 115 \text{ GeV}$. Notice that the ATLAS and CMS analyses [53–55, 68–71] employ similar cuts. We assume a detection efficiency of 99% (95%) for muons (electrons) that satisfy the event selections. These efficiencies correspond to those reported in the latest ATLAS analysis of off-shell Higgs production [55]. As input parameters we use $G_F = 1/(\sqrt{2}v^2) = 1.16639 \cdot 10^{-5} \text{ GeV}^{-2}$, $m_Z = 91.1876 \text{ GeV}$, $m_h = 125 \text{ GeV}$ and $m_t = 173 \text{ GeV}$. We employ NNPDF40_nlo_as_01180 parton distribution functions (PDFs) [72] with the renormalisation and factorisation scales μ_R and μ_F set to $m_{4\ell}$ on an event-by-event basis. Both the different-flavour $e^+e^-\mu^+\mu^-$ and the same-flavour $2e^+2e^-$ and $2\mu^+2\mu^-$ decay channels of the two Z bosons are included throughout our work.

In Figure 2 we show our predictions for the $m_{4\ell}$ distributions in the SM (dashed black) and three Higgs portal models (1.1). The displayed BSM benchmarks correspond to scalar masses of $m_\phi = 70 \text{ GeV}$ (solid red), $m_\phi = 100 \text{ GeV}$ (solid blue) and $m_\phi = 150 \text{ GeV}$ (solid green) assuming in all cases a coupling strength of $c_\phi = 3$. Notice that the chosen value of c_ϕ is safely below the limit $|c_\phi| < 4\pi$ following from perturbative tree-level unitarity (see for instance [34]). In the left panel the QCD-improved predictions for $gg \rightarrow ZZ \rightarrow 4\ell$ production including the Higgs signal, the continuum background and their interference are given. Two features of the shown BSM spectra deserve a further discussion. First, one observes peak-like structures in the distributions slightly above the threshold $m_{4\ell} = 2m_\phi$ of two-scalar production. Second, both spectra show an enhancement at large $m_{4\ell}$ because in the limit of partonic centre-of-mass energies $\hat{s} \rightarrow \infty$ the correction simplifies to $\Sigma(\hat{s}) - \delta m_h^2 \simeq -v^2|c_\phi|^2/(8\pi^2) \ln(\hat{s}/m_h^2)$. This behaviour is easily derived from (2.2). Notice furthermore that the $gg \rightarrow h^* \rightarrow ZZ \rightarrow 4\ell$ amplitudes interfere destructively with the $gg \rightarrow ZZ \rightarrow 4\ell$ matrix elements so that the overall sign of the correction $\Sigma(\hat{s}) - \delta m_h^2$ is effectively flipped. One also sees that for the three chosen sets of Higgs portal parameters the relative corrections in the spectra amount to less than 15% over the whole range of $m_{4\ell}$ values of interest. The same features are also observed in the right panel of Figure 2 which shows the corresponding predictions for $pp \rightarrow ZZ \rightarrow 4\ell$ production. Notice that in this case the relative modifications are smaller by a factor of roughly 10 than for $gg \rightarrow ZZ \rightarrow 4\ell$ due to the addition of the $q\bar{q} \rightarrow ZZ \rightarrow 4\ell$ channel which receives no BSM correction.

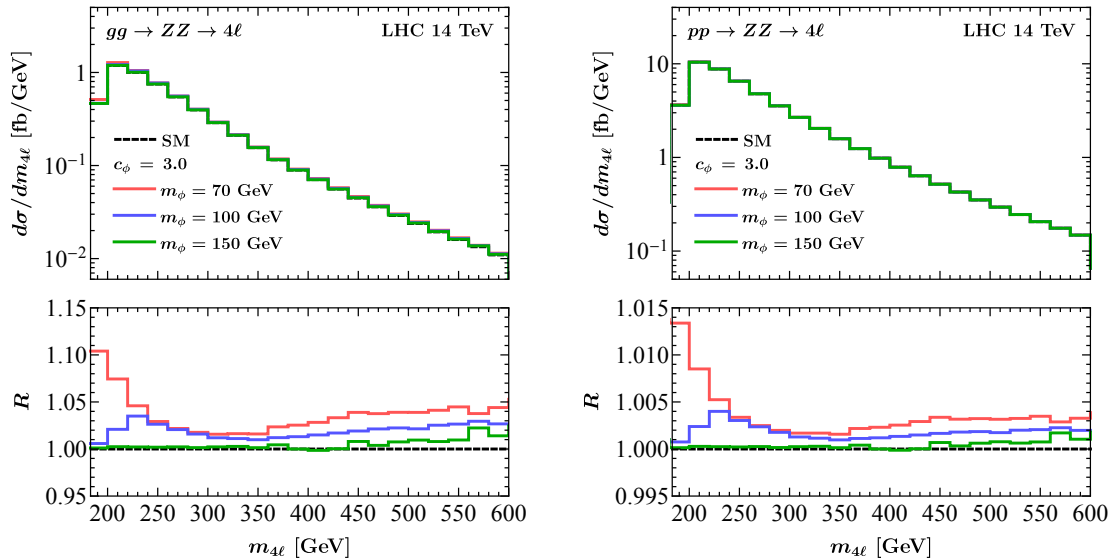


Figure 2: $m_{4\ell}$ spectra in the SM (dashed black) as well as for three Higgs portal model scenarios (1.1) assuming $c_\phi = 3$ and $m_\phi = 70$ GeV (solid red), $m_\phi = 100$ GeV (solid blue) and $m_\phi = 150$ GeV (solid green). The left (right) plot shows results for $gg \rightarrow ZZ \rightarrow 4\ell$ ($pp \rightarrow ZZ \rightarrow 4\ell$) production. All distributions correspond to QCD-improved predictions and LHC collisions at a centre-of-mass energy of $\sqrt{s} = 14$ TeV. The lower panels depict the ratios between the BSM distributions and the corresponding SM predictions.

To illustrate the discriminating power of the ME-based kinematic variable introduced in (3.1) we present in Figure 3 the results for the D_S spectra in the SM and beyond. The shown predictions have been obtained by means of (3.2) and the choices for the Higgs portal model parameters are those from before, apart from $m_\phi = 70$ GeV which is replaced by $m_\phi = 200$ GeV. One observes that compared to the SM spectrum the BSM distributions are shifted to lower values of D_S . This is a simple consequence of the fact that the correction $\Sigma(\hat{s}) - \delta m_h^2$ tends to reduce the $gg \rightarrow h^* \rightarrow ZZ \rightarrow 4\ell$ amplitude and thus P_h in (3.1). As a result of the sharp cut-off of the SM distribution at $D_S \simeq -3.5$, the relative BSM effects in the D_S spectra for $gg \rightarrow ZZ \rightarrow 4\ell$ turn out to be large, easily exceeding 100% for the chosen benchmark values of c_ϕ and m_ϕ . As illustrated in the right panel of Figure 3, adding the $q\bar{q} \rightarrow ZZ \rightarrow 4\ell$ channel to the predictions for the D_S distributions notably reduces the relative size of the Higgs portal corrections. Still assuming $c_\phi = 3$, the BSM effects reach the level of around 200%, 10% and 5% in the case of $m_\phi = 100$ GeV, $m_\phi = 150$ GeV and $m_\phi = 200$ GeV, respectively.

By comparing the relative modifications in the right panels of Figures 2 and 3 it should be already clear that the four-lepton invariant mass $m_{4\ell}$ has a much weaker discriminating power than the variable D_S in constraining interactions of the form (1.1). In order to make this statement quantitative we perform a shape analysis of both the $m_{4\ell}$ and D_S spectrum following the method outlined in our earlier work [49]. Specifically, the significance Z_i is

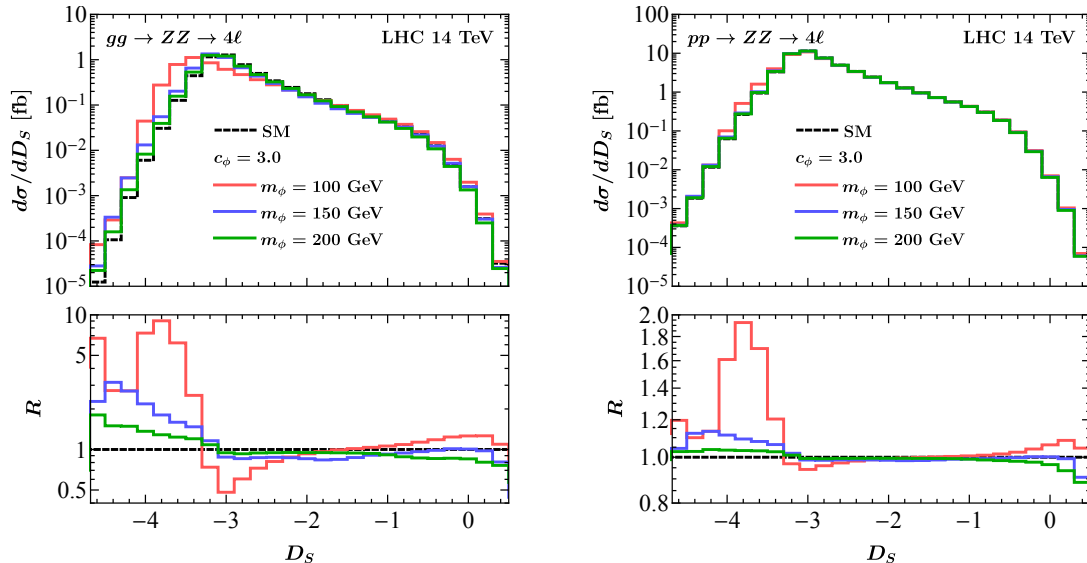


Figure 3: As Figure 2 but for the QCD-improved ME-based discriminant D_S as defined in (3.1) and (3.2). Furthermore, instead of $m_\phi = 70$ GeV a mass of $m_\phi = 200$ GeV is employed. For additional explanations see main text.

calculated as a Poisson ratio of likelihoods modified to incorporate systematic uncertainties on the background using the Asimov approximation [73]:

$$Z_i = \left\{ 2 \left[(s_i + b_i) \ln \left[\frac{(s_i + b_i)(b_i + \sigma_{b_i}^2)}{b_i^2 + (s_i + b_i)\sigma_{b_i}^2} \right] - \frac{b_i^2}{\sigma_{b_i}^2} \ln \left(1 + \frac{s_i \sigma_{b_i}^2}{b_i(b_i + \sigma_{b_i}^2)} \right) \right] \right\}^{1/2}. \quad (4.1)$$

Here s_i (b_i) represents the expected number of signal (background) events in bin i of the $m_{4\ell}$ or D_S spectrum and σ_{b_i} denotes the standard deviation that characterises the systematic uncertainties of the associated background in that bin. To set bounds on c_ϕ as a function of m_ϕ we assume that the central values of a future measurements of the two relevant distributions will line up with the SM predictions. We hence employ

$$s_i = N_i(c_\phi) - N_i(0), \quad b_i = N_i(0), \quad \sigma_{b_i} = \Delta_i N_i(0). \quad (4.2)$$

The total significance Z is obtained by adding the individual Z_i values in quadrature. Parameter regions with a total significance of $Z > \sqrt{2} \text{erf}^{-1}(\text{CL})$ are said to be excluded at a given confidence level CL. Here $\text{erf}^{-1}(z)$ denotes the inverse error function. In our shape analyses, we consider 23 bins of size of 20 GeV with four-lepton invariant masses in the range $140 \text{ GeV} < m_{4\ell} < 600 \text{ GeV}$ and 27 bins of equal size of 0.2 that cover the range $-4.9 < D_S < 0.5$ in the case of $m_{4\ell}$ and D_S , respectively.

A crucial ingredient in our analysis will turn out to be the systematic uncertainties σ_{b_i} on the background as parametrised by the parameters Δ_i in (4.2). In the case of the HL-LHC shape fits, we will employ the two different choices $\Delta_i = \Delta = 8\%$ and $\Delta_i = \Delta = 4\%$

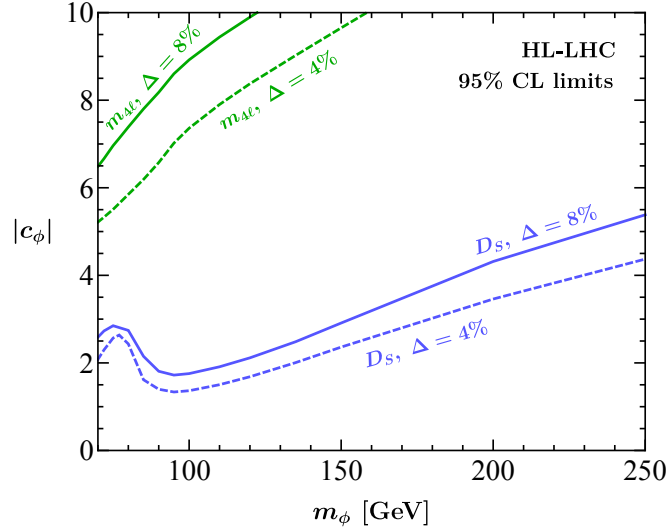


Figure 4: 95% CL limits on $|c_\phi|$ as a function of m_ϕ derived from the binned-likelihood analysis of the $m_{4\ell}$ (green lines) and the D_S (blue lines) spectrum at the HL-LHC. The solid (dashed) curves are obtained assuming a systematic uncertainty of $\Delta = 8\%$ ($\Delta = 4\%$). See main text for additional details.

of bin-independent systematic uncertainties. These choices can be motivated by recalling that the systematic uncertainties that ATLAS quotes in the HL-LHC study [74] for the on-shell $gg \rightarrow h \rightarrow ZZ$ signal strength amount to 5.0% and 3.9% in the baseline scenario S1 and S2 for the expected total systematic uncertainties. The corresponding systematic uncertainties quoted in the CMS work [69] are 7.3% and 4.1%. Since the dominant Higgs portal corrections in D_S are associated to kinematic configurations with $m_{4\ell}$ around $2m_\phi$, we believe that for not too heavy ϕ , theoretical predictions of the D_S spectra will reach an accuracy that is very similar to the systematics that is expected to be achievable at the HL-LHC in the case of on-shell $gg \rightarrow h \rightarrow ZZ$ production. Notice that the BSM effects in the $m_{4\ell}$ spectrum also receive important corrections in the region $m_{4\ell} > 2m_\phi$ as can be seen from the plots in Figure 2. Given the limitations (cf. [60, 75, 76]) of the state-of-the-art SM predictions of $pp \rightarrow ZZ$ production for kinematic configurations above the two top-quark threshold, achieving the assumed systematic uncertainties of $\Delta = 8\%$ and $\Delta = 4\%$ is certainly more challenging in the case of the $m_{4\ell}$ distribution. The steady progress of perturbative QCD calculations, in particular the exact evaluations of the two-loop on-shell amplitudes for $gg \rightarrow ZZ$ involving top quarks [77, 78] makes us, however, confident that systematic uncertainties in the ballpark of 10% or below are attainable till 3 ab^{-1} of data are collected at the HL-LHC.

The plot in Figure 4 displays the results of our binned-likelihood analysis when applied to the $m_{4\ell}$ (green lines) and the D_S (blue lines) distribution. Given the strong constraints on c_ϕ from on-shell Higgs boson decays into invisible [17–21] or undetected [4, 12] final states, we only consider m_ϕ values above the Higgs threshold at $m_h/2$. The shown 95% CL limits

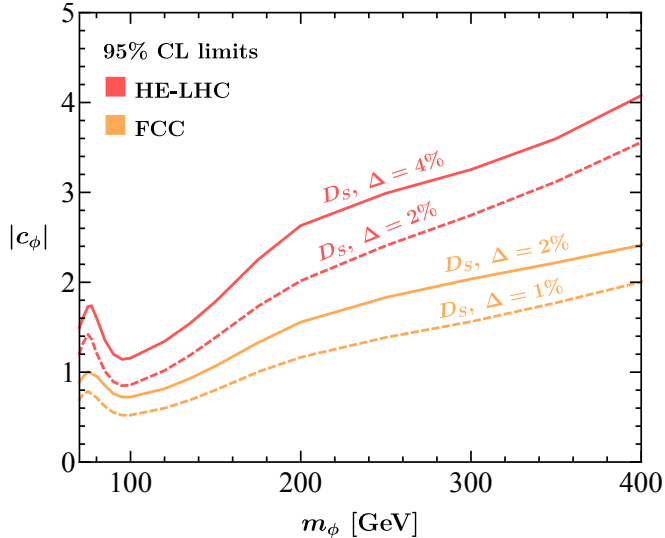


Figure 5: 95% CL limits on $|c_\phi|$ as a function of m_ϕ derived from the binned-likelihood analysis of the ME-based kinematic discriminant D_S . The red and orange exclusions illustrate our HE-LHC and FCC projections, respectively. The systematic uncertainties that have been assumed to obtain the different bounds are shown next to the lines and vary between $\Delta = 4\%$ and $\Delta = 1\%$. Further details are given in the main text.

correspond to our HL-LHC projections assuming the full expected integrated luminosity of 3 ab^{-1} at $\sqrt{s} = 14 \text{ TeV}$. The solid (dashed) exclusion lines have been obtained for a systematic uncertainty of $\Delta = 8\%$ ($\Delta = 4\%$). As anticipated, the exclusions that derive from the binned-likelihood analysis of the $m_{4\ell}$ spectrum are significantly weaker than those that follow from the D_S distribution. It is also evident from the figure that the size of the assumed systematic uncertainties plays a non-negligible role in the extraction of the 95% CL limits in the m_ϕ - $|c_\phi|$ plane, in particular, if the $m_{4\ell}$ spectrum is used to discriminate between the BSM signal and the SM background. We elaborate on this point further in Appendix A. In this context, we also add that our bounds following from the binned-likelihood analysis of the $m_{4\ell}$ distribution agree roughly with the HL-LHC limits presented in [41, 42] if one takes into account that these articles have considered the complex Higgs portal $|H|^2|\Phi|^2$. A thorough comparison with the latter results is however not possible because a discussion of systematic uncertainties is missing in the works [41, 42]. Notice finally that the bounds on $|c_\phi|$ that follow from our D_S likelihood-analysis have a non-trivial behaviour for $m_\phi \lesssim 100 \text{ GeV}$. This feature is related to the interference between the BSM signal and the SM background.

5 HE-LHC and FCC analyses

In the following we repeat the numerical analysis performed at the end of the last section for the HE-LHC and the FCC. In the case of the HE-LHC (FCC) we assume a

centre-of-mass energy of $\sqrt{s} = 27 \text{ TeV}$ ($\sqrt{s} = 100 \text{ TeV}$) and an integrated luminosity of 15 ab^{-1} (30 ab^{-1}). Apart from the $m_{4\ell}$ window which we enlarge to 1000 GeV (1500 GeV) at the HE-LHC (FCC), the selection cuts and detection efficiencies in our HE-LHC and FCC $pp \rightarrow ZZ \rightarrow 4\ell$ analyses resemble the ones spelled out at the beginning of Section 4. Possible reductions of the statistical uncertainties due to improvements in the HE-LHC and FCC detectors such as extended pseudorapidity coverages [79, 80] are not considered in our numerical analysis. We also take the values of the K -factors quoted in Section 3 that have been obtained for LHC collisions to calculate QCD-improved predictions for the kinematic variable D_S in (3.2). In view of the fact that the assumed systematic uncertainties largely determine the HE-LHC and FCC reach in constraining Higgs portal interactions of the form (1.1), we believe that these simplifications are fully justified. Moreover, since we have seen at the end of the last section that the ME-based kinematic discriminant D_S offers a significantly better sensitivity compared to $m_{4\ell}$, we will below only consider the former observable when determining the disfavoured regions in the $m_\phi - |c_\phi|$ plane.

The HE-LHC and FCC results of our shape fit to the D_S distribution are displayed in Figure 5. Like in the case of the HL-LHC we show results assuming different baseline scenarios for the assumed systematic uncertainties. In the case of the HE-LHC we employ $\Delta = 4\%$ and $\Delta = 2\%$, while in our FCC analysis we use $\Delta = 2\%$ and $\Delta = 1\%$. These systematic uncertainties can be motivated by noticing that the systematic uncertainties at the HE-LHC should be at least as small as those expected ultimately at the HL-LHC and that the FCC has a target precision of 1.8% for the $pp \rightarrow ZZ \rightarrow 4\ell$ channel [81]. Envisaging further theoretical and experimental progress a final systematic uncertainty of 1% at the FCC does therefore not seem inconceivable. From the different curves one again sees that the size of the assumed systematic uncertainties plays a notable role in determining the collider reach. Numerically, we find that halving the systematic uncertainties at the HE-LHC (FCC) leads to improvements of the 95% CL bounds on $|c_\phi|$ of around 25% (30%) at $m_\phi \simeq 100 \text{ GeV}$ and about 20% (25%) at $m_\phi \simeq 250 \text{ GeV}$. The gain in statistical power of the FCC compared to the HE-LHC is however also visible from the figure with the FCC bound at $m_\phi \simeq 250 \text{ GeV}$ being better by roughly 25% than that of the HE-LHC assuming the same systematic uncertainties of $\Delta = 2\%$. This trend continues at higher values of the real scalar mass reaching up to almost 35% at $m_\phi \simeq 400 \text{ GeV}$.

6 Discussion and outlook

In Figure 6 we compare the HL-LHC reach of different search strategies in the $m_\phi - |c_\phi|$ plane. The solid blue exclusion line corresponds to the 95% CL limits that derives from the proposed binned-likelihood analysis of the ME-based kinematic discriminant D_S assuming a systematic uncertainty of $\Delta = 4\%$. The solid green line instead indicates the bound obtained in [32] from a study of off-shell Higgs production in the VBF channel. This analysis assumes a systematic uncertainty of $\Delta = 1\%$. At the HL-LHC, measurements of the global Higgs signal strength μ_h are expected to reach an accuracy of $\Delta = 2.4\%$ in the baseline scenario S2 for the expected total systematic uncertainties [74]. Utilising the quoted precision together with (2.2) and (2.3) leads at 95% CL to the solid red line. Another process

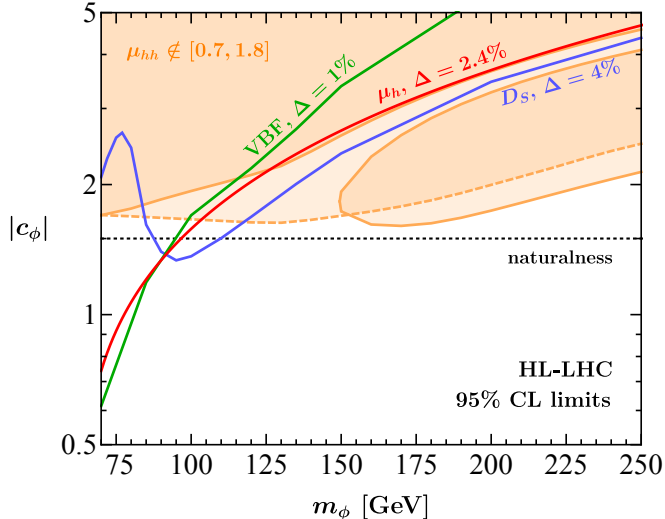


Figure 6: Comparison of the HL-LHC reach of different search strategies in the m_ϕ - $|c_\phi|$ plane. The solid blue, solid green and solid red line correspond to the 95% CL limits that derive from our binned-likelihood analysis of the ME-based kinematic discriminant D_S , the VBF analysis performed in [32] and a hypothetical measurement of the global Higgs signal strength μ_h , respectively. If applicable the assumed systematic uncertainties or accuracies are indicated. The parameter spaces above the coloured lines are disfavoured. The region bounded by the solid (dashed) orange line follows from imposing that the signal strength in double-Higgs production obeys $\mu_{hh} \notin [0.7, 1.8]$ for $c_\phi > 0$ ($c_\phi < 0$). The dotted black line corresponds to the bound $|c_\phi| = \sqrt{3}y_t^2 = 1.5$ that derives from naturalness arguments in models of neutral naturalness. For more details see main text.

that is sensitive to Higgs portal interactions of the form (1.1) is double-Higgs production as previously demonstrated in [28, 32, 39, 40, 43]. The 95% CL bound $\kappa_\lambda \in [0.18, 3.6]$ on the modifications $\kappa_\lambda = \lambda/\lambda_{\text{SM}}$ with $\lambda_{\text{SM}} = m_h^2/(2v^2) \simeq 0.13$ of the trilinear Higgs coupling as found by the CMS projection [82] implies $\mu_{hh} \in [0.7, 1.8]$ on the signal strength in double-Higgs production at the HL-LHC. By implementing the full one-loop corrections due to (1.1) into MCFM and imposing the latter bound we obtain the solid and dashed orange lines. Consult Appendix B for further details. Finally, the dashed black line corresponds to the naturalness bound $|c_\phi| = \sqrt{3}y_t^2 = 1.5$ discussed in Section 1.

From Figure 6 it is evident that for $m_\phi \lesssim 90$ GeV the VBF and μ_h projections provide nominally the best constraints at the HL-LHC. In the case of $m_\phi \gtrsim 90$ GeV, on the other hand, double-Higgs production at the HL-LHC typically allows to set the most stringent constraints on the parameters appearing in (1.1). Notice also that the D_S constraint provides the best sensitivity for $90 \text{ GeV} \lesssim m_\phi \lesssim 120$ GeV and stronger constraints than VBF and μ_h for $m_\phi \gtrsim 90$ GeV. The fact that the constraints that stem from double-Higgs production are not symmetric under $c_\phi \leftrightarrow -c_\phi$ is readily understood by noting that the Higgs portal corrections to the $gg \rightarrow hh$ amplitude involve both terms proportional to c_ϕ^3 and c_ϕ^2 .

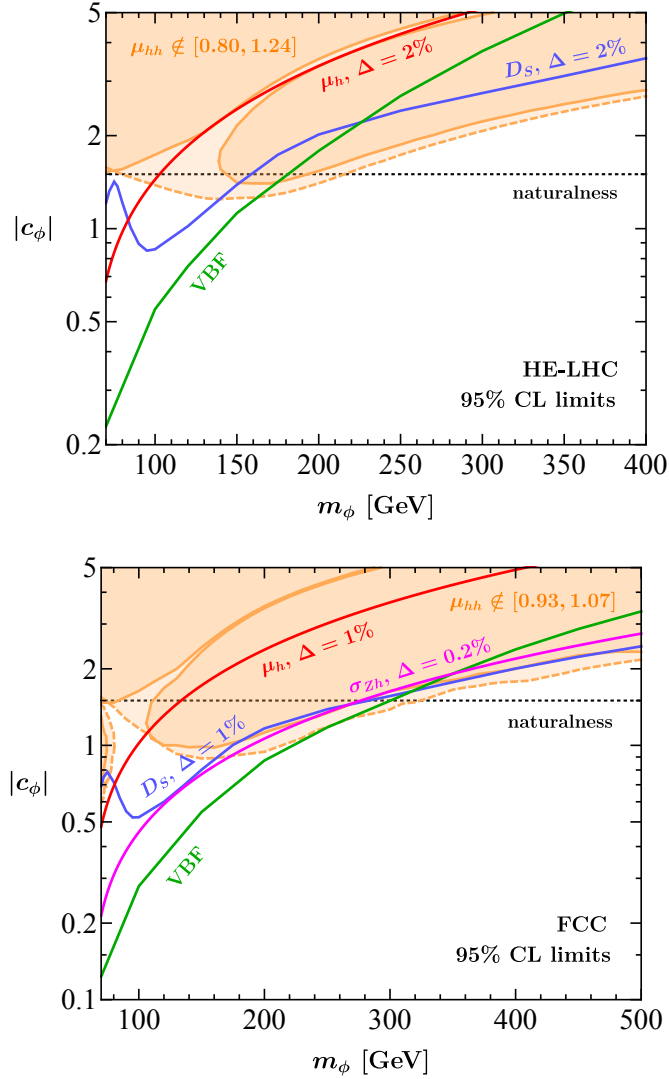


Figure 7: Comparison of the HE-LHC (upper panel) and FCC (lower panel) reach of different search strategies in the $m_\phi - |c_\phi|$ plane. Besides the constraints shown in Figure 6 also the 95% CL limit that follows from a precision measurement of the Zh production cross section σ_{Zh} is displayed in the case of the FCC as a solid magenta line. The colour coding and meaning of the other constraints resembles those in the former figure. Consult the main text for additional explanations.

In fact, integrating out the real scalar ϕ leads to the following one-loop modification of the trilinear Higgs coupling (see for instance [32, 83]):

$$\kappa_\lambda \simeq 1 + \frac{v^2 c_\phi^2}{12\pi^2 m_\phi^2} \left(\frac{v^2 c_\phi}{m_h^2} - \frac{7}{12} \right), \quad (6.1)$$

where the terms in brackets interfere destructively (constructively) for $c_\phi > 0$ ($c_\phi < 0$). We

add that the numerical value of the second term in brackets depends on the definition and the kinematics of the trilinear Higgs vertex and that the value in (6.1) is obtained from the full one-loop form factor (B.2) assuming two on-shell external Higgs bosons. The intricate dependence of the $gg \rightarrow hh$ amplitude on m_ϕ and c_ϕ also leads in the case of $c_\phi > 0$ to the island of disfavoured parameters starting at $m_\phi \simeq 145$ GeV and $c_\phi \simeq 1.7$. This point is discussed in more detail in Appendix B. Notice furthermore that all constraints shown in Figure 6 depend in a non-negligible way on the assumed systematic uncertainties or accuracies. Finally, the VBF limit only applies if the new degrees of freedom produced in $h^* \rightarrow \phi\phi$ are collider stable and thus lead to a missing transverse energy (E_T^{miss}) signal at the HL-LHC. In view of these caveats one can conclude that to fully exploit the HL-LHC potential in probing Higgs portal interactions of the form (1.1) one should consider all direct and indirect probes displayed in Figure 6. But even in such a case one sees that at the HL-LHC only theories compatible with the naturalness bound can be explored if the new particles that cancel the quadratic sensitivity of the Higgs mass are not heavier than $m_\phi \simeq 110$ GeV.

In the case of the HE-LHC and the FCC the sensitivity of the different search strategies to the Higgs portal parameters is shown in the two panels of Figure 7. The displayed D_S constraints assume systematic uncertainties of $\Delta = 2\%$ and $\Delta = 1\%$, while the VBF limits taken from [32] include only statistical uncertainties. In the case of the global Higgs signal strength μ_h , we employ $\Delta = 2\%$ and $\Delta = 1\%$ [81]. The 95% CL bounds on modifications of the trilinear Higgs coupling at the HE-LHC and the FCC are expected to be $\kappa_\lambda \in [0.7, 1.3]$ and $\kappa_\lambda \in [0.9, 1.1]$, respectively. See for example [84–86] for detailed discussions. The corresponding two-sided limits on the signal strength in double-Higgs production are $\mu_{hh} \in [0.80, 1.24]$ and $\mu_{hh} \in [0.93, 1.07]$. In addition, we show in the case of the FCC the exclusion that follows from an extraction of the Zh cross section σ_{Zh} with an accuracy of $\Delta = 0.2\%$ as a solid magenta line. Such a precision measurement should be possible at the e^+e^- predecessor of the FCC running at a centre-of-mass energy of $\sqrt{s} = 240$ GeV with an integrated luminosity of 5 ab^{-1} [87]. The overall picture observed at the HE-LHC is very similar to that seen at the HL-LHC. Nominal the strongest constraint arises for $m_\phi \lesssim 170$ GeV ($m_\phi \gtrsim 170$ GeV) from VBF off-shell Higgs (double-Higgs) production, but the D_S constraint also provides complementary sensitivity in particular for higher values of m_ϕ . In the case of the FCC, one furthermore observes that a high precision measurement of σ_{Zh} can provide additional relevant bounds in the m_ϕ - $|c_\phi|$ plane. The combination of all constraints shown in the panels of Figure 7 should allow to probe natural BSM theories of the form (1.2) if the new particles that cancel the quadratic sensitivity of the Higgs mass appear below approximately $m_\phi \simeq 200$ GeV ($m_\phi \simeq 300$ GeV) at the HE-LHC (FCC).

We add that the potential of CLIC and a muon collider in constraining Higgs portal interactions of the form (1.1) through VBF off-shell Higgs production has been studied in the article [32]. See also [23, 24, 26, 30] for similar analyses concerning the reach of future lepton colliders. While CLIC is not expected to improve the FCC bounds shown in the lower panel of Figure 7 even when running at a centre-of-mass energy of $\sqrt{s} = 3$ TeV and collecting 3 ab^{-1} of data, a muon collider with $\sqrt{s} = 6$ TeV and 6 ab^{-1} ($\sqrt{s} = 14$ TeV and 14 ab^{-1}) should allow to test natural theories of neutral naturalness up to $m_\phi \simeq$

500 GeV ($m_\phi \simeq 900$ GeV) thereby exceeding (significantly) the FCC reach.

Acknowledgments

We thank Maximilian Ruhdorfer, Ennio Salvioni and Andreas Weiler for useful discussions, for helpful comments on the manuscript and for providing us with the limits of their VBF analysis [32] in electronic form. The Max Planck Computing and Data Facility (MPCDF) in Garching has been used to carry out the MC simulations related to this work. Our computations made use of the `Mathematica` packages `FeynRules` [88], `FeynArts` [89], `FormCalc` [50, 51] and `Package-X` [90].

A Systematic uncertainties

In this appendix we discuss in more detail the prospects of the proposed binned-likelihood analyses of the D_S spectra for the HL-LHC, the HE-LHC and the FCC. In particular, we examine how different assumptions on the systematic uncertainties affect the resulting constraints on the parameter space of the Higgs portal model (1.1). In Figure 8, we show the projected 95% CL limits on $|c_\phi|$ derived from our D_S analysis as a function of the assumed systematic uncertainty Δ for the three aforementioned colliders. The presented limits are obtained using the benchmark numerical values for the scalar masses indicated in the figure that vary between $100 \text{ GeV} \leq m_\phi \leq 200 \text{ GeV}$.

Figure 8 further illustrates the point already made in Sections 4 and 5, that the assumptions on the systematic uncertainties Δ play a crucial role in constraining the m_ϕ - $|c_\phi|$ parameter space by using the D_S distribution as a kinematic discriminant. In particular, one observes that the enhanced statistical power provided by the HE-LHC and the FCC, which results from the increased centre-of-mass energy and integrated luminosity of these machines compared to the HL-LHC, can only be fully exploited if systematic uncertainties are under control. For instance, in the case of $m_\phi = 100$ GeV the sensitivity gain between the HL-LHC and the FCC is around 17% for $\Delta = 20\%$, while for $\Delta = 1\%$ the improvement amounts to about 41%. Similar numbers of approximately 26% and 51% are found for $m_\phi = 150$ GeV and $m_\phi = 200$ GeV, implying that the gain in sensitivity between different colliders is to first approximation mass-independent for the low values of m_ϕ considered in the figure.

B Details of the double-Higgs calculation

At the one-loop level the $gg \rightarrow hh$ process receives contributions from virtual ϕ exchange in propagator and vertex diagrams as well as counterterm contributions associated to wave function, mass and tadpole renormalisation (see [39, 43] for details). In the on-shell scheme the combined corrections involving the Wilson coefficient c_ϕ can be written as a finite shift:

$$\lambda_{\text{SM}} \rightarrow \lambda_{\text{SM}} [1 + \delta(\hat{s})]. \quad (\text{B.1})$$

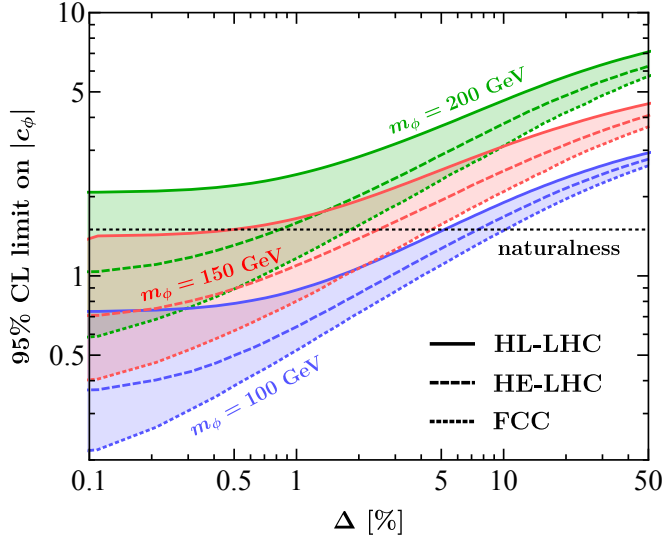


Figure 8: 95% CL limits on $|c_\phi|$ derived from the binned-likelihood analysis of the D_S spectra as a function of the assumed systematic uncertainty Δ . The bounds for the HL-LHC (solid lines), the HE-LHC (dashed lines) and the FCC (dotted lines) are displayed for the three benchmark values $m_\phi = 100$ GeV (blue), $m_\phi = 150$ GeV (red) and $m_\phi = 200$ GeV (green) of the scalar mass. The dotted black line corresponds to the condition $|c_\phi| = \sqrt{3}y_t^2 = 1.5$ that derives from naturalness arguments in models of neutral naturalness. See main text for additional details.

Here $\lambda_{\text{SM}} = m_h^2/(2v^2)$ is the tree-level expression for the trilinear Higgs coupling in the SM and the \hat{s} -dependent form factor is given by

$$\begin{aligned} \delta(\hat{s}) = & -\frac{v^2 c_\phi^2}{24\pi^2 m_h^2} \left(1 + \frac{3m_h^2}{\hat{s} - m_h^2}\right) \left[B_0(\hat{s}, m_\phi^2, m_\phi^2) - B_0(m_h^2, m_\phi^2, m_\phi^2) \right] \\ & - \frac{v^4 c_\phi^3}{6\pi^2 m_h^2} C_0(m_h^2, m_h^2, \hat{s}, m_\phi^2, m_\phi^2, m_\phi^2) - \frac{v^2 c_\phi^2}{8\pi^2} \frac{d}{d\hat{s}} B_0(\hat{s}, m_\phi^2, m_\phi^2) \Big|_{\hat{s}=m_h^2}, \end{aligned} \quad (\text{B.2})$$

with the A_0 , B_0 and C_0 functions are one-, two-, and three-point Passarino-Veltman scalar integrals defined as in [50, 51]. Our result (B.2) agrees with [39, 43], after fixing a sign error in (12) of [43]. Notice that after integrating out the scalar field ϕ by expanding the on-shell form factor $\delta(2m_h^2)$ up to the first power in m_h^2/m_ϕ^2 , one recovers the approximate correction for κ_λ as given in (6.1).

To obtain predictions for double-Higgs production we have implemented the analytic results (B.2) at the amplitude level into MCFM. We then perform sensitivity scans in the parameters c_ϕ and m_ϕ , using the setup discussed at the beginning of Section 4, but fixing the renormalisation and factorisation scales μ_R and μ_F to the value $2m_h$. In Figure 9 we show results for the signal strength μ_{hh} in double-Higgs production for three different values of m_ϕ as a function of c_ϕ . The displayed curves correspond to the results obtained at the FCC.

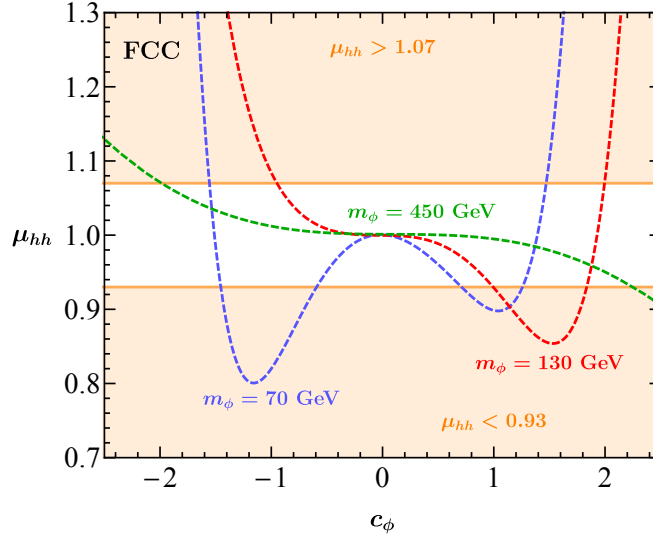


Figure 9: The signal strength for double-Higgs production (μ_{hh}) at the FCC as a function of the Wilson coefficient c_ϕ for three values of the scalar mass: $m_\phi = 70$ GeV (dashed blue), $m_\phi = 130$ GeV (dashed red) and $m_\phi = 450$ GeV (dashed green). The regions excluded by the projected experimental constraint $\mu_{hh} \in [0.93, 1.07]$ are shown in orange. For further explanations see main text.

Two features of the shown predictions deserve some comments. First, due to the c_ϕ^3 and c_ϕ^2 dependence of (B.2) the signal strengths μ_{hh} are not symmetric under $c_\phi \leftrightarrow -c_\phi$. Second, the functional form of μ_{hh} depends also sensitively on the mass m_ϕ . For low ϕ masses as illustrated by the choice $m_\phi = 70$ GeV in the figure, the signal strength μ_{hh} has two minima, one at around $c_\phi \simeq -1.1$ and another one at $c_\phi \simeq 1.0$. This feature leads to the orange exclusions in the lower plot in Figure 7 at $|c_\phi| \simeq 1$. For larger values of m_ϕ the signal strengths μ_{hh} have instead only a single minimum at positive values of c_ϕ . Notice that if the value of μ_{hh} at this minimum is incompatible with the experimental allowed range, such as happens to be the case for example for $m_\phi = 130$ GeV at the FCC, increasing/decreasing the value of c_ϕ will always result in μ_{hh} values that are consistent with experiment. This feature leads to the orange exclusions shown in the plots of Figures 6 and 7 that are relevant for $c_\phi > 0$ and separated by a funnel of viable solutions.

References

- [1] ATLAS collaboration, *Observation of a new particle in the search for the Standard Model Higgs boson with the ATLAS detector at the LHC*, *Phys. Lett. B* **716** (2012) 1 [1207.7214].
- [2] CMS collaboration, *Observation of a New Boson at a Mass of 125 GeV with the CMS Experiment at the LHC*, *Phys. Lett. B* **716** (2012) 30 [1207.7235].
- [3] CMS collaboration, *Combined Higgs boson production and decay measurements with up to 137 fb⁻¹ of proton-proton collision data at $\sqrt{s} = 13$ TeV*, CMS-PAS-HIG-19-005, CERN,

Geneva (2020).

- [4] ATLAS collaboration, *A combination of measurements of Higgs boson production and decay using up to 139 fb^{-1} of proton-proton collision data at $\sqrt{s} = 13 \text{ TeV}$ collected with the ATLAS experiment*, *ATLAS-CONF-2020-027*, CERN, Geneva (2020).
- [5] V. Silveira and A. Zee, *Scalar Phantoms*, *Phys. Lett. B* **161** (1985) 136.
- [6] J. McDonald, *Gauge singlet scalars as cold dark matter*, *Phys. Rev. D* **50** (1994) 3637 [[hep-ph/0702143](#)].
- [7] C.P. Burgess, M. Pospelov and T. ter Veldhuis, *The Minimal model of nonbaryonic dark matter: A Singlet scalar*, *Nucl. Phys. B* **619** (2001) 709 [[hep-ph/0011335](#)].
- [8] B. Patt and F. Wilczek, *Higgs-field portal into hidden sectors*, [[hep-ph/0605188](#)].
- [9] V. Barger, P. Langacker, M. McCaskey, M.J. Ramsey-Musolf and G. Shaughnessy, *LHC Phenomenology of an Extended Standard Model with a Real Scalar Singlet*, *Phys. Rev. D* **77** (2008) 035005 [[0706.4311](#)].
- [10] G. Arcadi, A. Djouadi and M. Raidal, *Dark Matter through the Higgs portal*, *Phys. Rept.* **842** (2020) 1 [[1903.03616](#)].
- [11] O. Lebedev, *The Higgs portal to cosmology*, *Prog. Part. Nucl. Phys.* **120** (2021) 103881 [[2104.03342](#)].
- [12] S. Argyropoulos, O. Brandt and U. Haisch, *Collider Searches for Dark Matter through the Higgs Lens*, *Symmetry* **2021** (2021) 13 [[2109.13597](#)].
- [13] E. Hardy, *Higgs portal dark matter in non-standard cosmological histories*, *JHEP* **06** (2018) 043 [[1804.06783](#)].
- [14] D. Curtin and P. Saraswat, *Towards a No-Lose Theorem for Naturalness*, *Phys. Rev. D* **93** (2016) 055044 [[1509.04284](#)].
- [15] T. Cohen, N. Craig, G.F. Giudice and M. McCullough, *The Hyperbolic Higgs*, *JHEP* **05** (2018) 091 [[1803.03647](#)].
- [16] H.-C. Cheng, L. Li, E. Salvioni and C.B. Verhaaren, *Singlet Scalar Top Partners from Accidental Supersymmetry*, *JHEP* **05** (2018) 057 [[1803.03651](#)].
- [17] A. Djouadi, O. Lebedev, Y. Mambrini and J. Quevillon, *Implications of LHC searches for Higgs-portal dark matter*, *Phys. Lett. B* **709** (2012) 65 [[1112.3299](#)].
- [18] Y. Mambrini, *Higgs searches and singlet scalar dark matter: Combined constraints from XENON 100 and the LHC*, *Phys. Rev. D* **84** (2011) 115017 [[1108.0671](#)].
- [19] A. Djouadi, A. Falkowski, Y. Mambrini and J. Quevillon, *Direct Detection of Higgs-Portal Dark Matter at the LHC*, *Eur. Phys. J. C* **73** (2013) 2455 [[1205.3169](#)].
- [20] CMS collaboration, *Search for invisible decays of a Higgs boson produced through vector boson fusion in proton-proton collisions at $\sqrt{s} = 13 \text{ TeV}$* , *Phys. Lett. B* **793** (2019) 520 [[1809.05937](#)].
- [21] ATLAS collaboration, *Combination of searches for invisible Higgs boson decays with the ATLAS experiment*, *ATLAS-CONF-2020-052*, CERN, Geneva (2020).
- [22] E.W.N. Glover and J.J. van der Bij, *Vector boson pair production via gluon fusion*, *Phys. Lett. B* **219** (1989) 488.

- [23] S. Matsumoto, K. Fujii, T. Honda, S. Kanemura, T. Nabeshima, N. Okada et al., *Observing the Coupling between Dark Matter and Higgs Boson at the ILC*, in *International Linear Collider Workshop*, 6, 2010 [[1006.5268](#)].
- [24] S. Kanemura, S. Matsumoto, T. Nabeshima and H. Taniguchi, *Testing Higgs portal dark matter via Z fusion at a linear collider*, *Phys. Lett. B* **701** (2011) 591 [[1102.5147](#)].
- [25] N. Kauer and G. Passarino, *Inadequacy of zero-width approximation for a light Higgs boson signal*, *JHEP* **08** (2012) 116 [[1206.4803](#)].
- [26] Z. Chacko, Y. Cui and S. Hong, *Exploring a Dark Sector Through the Higgs Portal at a Lepton Collider*, *Phys. Lett. B* **732** (2014) 75 [[1311.3306](#)].
- [27] M. Endo and Y. Takaesu, *Heavy WIMP through Higgs portal at the LHC*, *Phys. Lett. B* **743** (2015) 228 [[1407.6882](#)].
- [28] D. Curtin, P. Meade and C.-T. Yu, *Testing Electroweak Baryogenesis with Future Colliders*, *JHEP* **11** (2014) 127 [[1409.0005](#)].
- [29] N. Craig, H.K. Lou, M. McCullough and A. Thalapillil, *The Higgs Portal Above Threshold*, *JHEP* **02** (2016) 127 [[1412.0258](#)].
- [30] P. Ko and H. Yokoya, *Search for Higgs portal DM at the ILC*, *JHEP* **08** (2016) 109 [[1603.04737](#)].
- [31] D. Buttazzo, D. Redigolo, F. Sala and A. Tesi, *Fusing Vectors into Scalars at High Energy Lepton Colliders*, *JHEP* **11** (2018) 144 [[1807.04743](#)].
- [32] M. Ruhdorfer, E. Salvioni and A. Weiler, *A Global View of the Off-Shell Higgs Portal*, *SciPost Phys.* **8** (2020) 027 [[1910.04170](#)].
- [33] J. Heisig, M. Krämer, E. Madge and A. Mück, *Probing Higgs-portal dark matter with vector-boson fusion*, *JHEP* **03** (2020) 183 [[1912.08472](#)].
- [34] C. Englert, J. Jaeckel, M. Spannowsky and P. Stylianou, *Power meets Precision to explore the Symmetric Higgs Portal*, *Phys. Lett. B* **806** (2020) 135526 [[2002.07823](#)].
- [35] A. Garcia-Abenza and J.M. No, *Shining light through the Higgs portal with $\gamma\gamma$ colliders*, [[2011.03551](#)].
- [36] U. Haisch, G. Polesello and S. Schulte, *Searching for pseudo Nambu-Goldstone boson dark matter production in association with top quarks*, *JHEP* **09** (2021) 206 [[2107.12389](#)].
- [37] C. Englert and M. McCullough, *Modified Higgs Sectors and NLO Associated Production*, *JHEP* **07** (2013) 168 [[1303.1526](#)].
- [38] N. Craig, C. Englert and M. McCullough, *New Probe of Naturalness*, *Phys. Rev. Lett.* **111** (2013) 121803 [[1305.5251](#)].
- [39] S.-P. He and S.-h. Zhu, *One-loop radiative correction to the triple Higgs coupling in the Higgs singlet model*, *Phys. Lett. B* **764** (2017) 31 [[1607.04497](#)].
- [40] S. Kanemura, M. Kikuchi and K. Yagyu, *One-loop corrections to the Higgs self-couplings in the singlet extension*, *Nucl. Phys. B* **917** (2017) 154 [[1608.01582](#)].
- [41] D. Gonçalves, T. Han and S. Mukhopadhyay, *Off-Shell Higgs Probe of Naturalness*, *Phys. Rev. Lett.* **120** (2018) 111801 [[1710.02149](#)].
- [42] D. Gonçalves, T. Han and S. Mukhopadhyay, *Higgs Couplings at High Scales*, *Phys. Rev. D* **98** (2018) 015023 [[1803.09751](#)].

- [43] C. Englert and J. Jaeckel, *Probing the Symmetric Higgs Portal with Di-Higgs Boson Production*, *Phys. Rev. D* **100** (2019) 095017 [[1908.10615](#)].
- [44] F. Caola and K. Melnikov, *Constraining the Higgs boson width with ZZ production at the LHC*, *Phys. Rev. D* **88** (2013) 054024 [[1307.4935](#)].
- [45] Y. Gao, A.V. Gritsan, Z. Guo, K. Melnikov, M. Schulze and N.V. Tran, *Spin Determination of Single-Produced Resonances at Hadron Colliders*, *Phys. Rev. D* **81** (2010) 075022 [[1001.3396](#)].
- [46] S. Bolognesi, Y. Gao, A.V. Gritsan, K. Melnikov, M. Schulze, N.V. Tran et al., *On the spin and parity of a single-produced resonance at the LHC*, *Phys. Rev. D* **86** (2012) 095031 [[1208.4018](#)].
- [47] I. Anderson et al., *Constraining Anomalous HVV Interactions at Proton and Lepton Colliders*, *Phys. Rev. D* **89** (2014) 035007 [[1309.4819](#)].
- [48] J.M. Campbell, R.K. Ellis and C. Williams, *Bounding the Higgs Width at the LHC Using Full Analytic Results for $gg \rightarrow e^-e^+\mu^-\mu^+$* , *JHEP* **04** (2014) 060 [[1311.3589](#)].
- [49] U. Haisch and G. Koole, *Off-shell Higgs production at the LHC as a probe of the trilinear Higgs coupling*, *JHEP* **02** (2022) 030 [[2111.12589](#)].
- [50] T. Hahn and M. Perez-Victoria, *Automatized one loop calculations in four-dimensions and D-dimensions*, *Comput. Phys. Commun.* **118** (1999) 153 [[hep-ph/9807565](#)].
- [51] T. Hahn, S. Paßehr and C. Schappacher, *FormCalc 9 and Extensions*, *PoS* **LL2016** (2016) 068 [[1604.04611](#)].
- [52] R. Boughezal, J.M. Campbell, R.K. Ellis, C. Focke, W. Giele, X. Liu et al., *Color singlet production at NNLO in MCFM*, *Eur. Phys. J. C* **77** (2017) 7 [[1605.08011](#)].
- [53] ATLAS collaboration, *Constraints on the off-shell Higgs boson signal strength in the high-mass ZZ and WW final states with the ATLAS detector*, *Eur. Phys. J. C* **75** (2015) 335 [[1503.01060](#)].
- [54] ATLAS collaboration, *Constraints on off-shell Higgs boson production and the Higgs boson total width in $ZZ \rightarrow 4\ell$ and $ZZ \rightarrow 2\ell 2\nu$ final states with the ATLAS detector*, *Phys. Lett. B* **786** (2018) 223 [[1808.01191](#)].
- [55] ATLAS collaboration, *Measurement of the four-lepton invariant mass spectrum in 13 TeV proton-proton collisions with the ATLAS detector*, *JHEP* **04** (2019) 048 [[1902.05892](#)].
- [56] F. Cascioli, T. Gehrmann, M. Grazzini, S. Kallweit, P. Maierhöfer, A. von Manteuffel et al., *ZZ production at hadron colliders in NNLO QCD*, *Phys. Lett. B* **735** (2014) 311 [[1405.2219](#)].
- [57] M. Grazzini, S. Kallweit and D. Rathlev, *ZZ production at the LHC: fiducial cross sections and distributions in NNLO QCD*, *Phys. Lett. B* **750** (2015) 407 [[1507.06257](#)].
- [58] G. Heinrich, S. Jahn, S.P. Jones, M. Kerner and J. Pires, *NNLO predictions for Z-boson pair production at the LHC*, *JHEP* **03** (2018) 142 [[1710.06294](#)].
- [59] S. Kallweit and M. Wiesemann, *ZZ production at the LHC: NNLO predictions for $2\ell 2\nu$ and 4ℓ signatures*, *Phys. Lett. B* **786** (2018) 382 [[1806.05941](#)].
- [60] L. Buonocore, G. Koole, D. Lombardi, L. Rottoli, M. Wiesemann and G. Zanderighi, *ZZ production at nNNLO+PS with MiNNLO_{PS}*, [[2108.05337](#)].
- [61] F. Caola, K. Melnikov, R. Röntsch and L. Tancredi, *QCD corrections to ZZ production in gluon fusion at the LHC*, *Phys. Rev. D* **92** (2015) 094028 [[1509.06734](#)].

- [62] F. Caola, M. Dowling, K. Melnikov, R. Röntsch and L. Tancredi, *QCD corrections to vector boson pair production in gluon fusion including interference effects with off-shell Higgs at the LHC*, *JHEP* **07** (2016) 087 [[1605.04610](#)].
- [63] M. Grazzini, S. Kallweit, M. Wiesemann and J.Y. Yook, *ZZ production at the LHC: NLO QCD corrections to the loop-induced gluon fusion channel*, *JHEP* **03** (2019) 070 [[1811.09593](#)].
- [64] M. Grazzini, S. Kallweit, M. Wiesemann and J.Y. Yook, *Four lepton production in gluon fusion: Off-shell Higgs effects in NLO QCD*, *Phys. Lett. B* **819** (2021) 136465 [[2102.08344](#)].
- [65] C. Anastasiou, C. Duhr, F. Dulat, F. Herzog and B. Mistlberger, *Higgs Boson Gluon-Fusion Production in QCD at Three Loops*, *Phys. Rev. Lett.* **114** (2015) 212001 [[1503.06056](#)].
- [66] M. Grazzini, S. Kallweit, J.M. Lindert, S. Pozzorini and M. Wiesemann, *NNLO QCD + NLO EW with Matrix+OpenLoops: precise predictions for vector-boson pair production*, *JHEP* **02** (2020) 087 [[1912.00068](#)].
- [67] F. Maltoni, D. Pagani, A. Shivaji and X. Zhao, *Trilinear Higgs coupling determination via single-Higgs differential measurements at the LHC*, *Eur. Phys. J. C* **77** (2017) 887 [[1709.08649](#)].
- [68] ATLAS collaboration, *Off-shell Higgs boson couplings measurement using $H \rightarrow ZZ \rightarrow 4l$ events at High Luminosity LHC*, [ATL-PHYS-PUB-2015-024](#), CERN, Geneva (2015).
- [69] CMS collaboration, *Sensitivity projections for Higgs boson properties measurements at the HL-LHC*, [CMS-PAS-FTR-18-011](#), CERN, Geneva (2018).
- [70] CMS collaboration, *Constraints on the Higgs boson width from off-shell production and decay to Z-boson pairs*, *Phys. Lett. B* **736** (2014) 64 [[1405.3455](#)].
- [71] CMS collaboration, *Measurements of the Higgs boson width and anomalous HVV couplings from on-shell and off-shell production in the four-lepton final state*, *Phys. Rev. D* **99** (2019) 112003 [[1901.00174](#)].
- [72] R.D. Ball et al., *The Path to Proton Structure at One-Percent Accuracy*, [[2109.02653](#)].
- [73] G. Cowan, K. Cranmer, E. Gross and O. Vitells, *Asymptotic formulae for likelihood-based tests of new physics*, *Eur. Phys. J. C* **71** (2011) 1554 [[1007.1727](#)].
- [74] ATLAS collaboration, *Projections for measurements of Higgs boson cross sections, branching ratios, coupling parameters and mass with the ATLAS detector at the HL-LHC*, [ATL-PHYS-PUB-2018-054](#), CERN, Geneva (2018).
- [75] S. Amoroso et al., *Les Houches 2019: Physics at TeV Colliders: Standard Model Working Group Report*, in *11th Les Houches Workshop on Physics at TeV Colliders: PhysTeV Les Houches*, 3, 2020 [[2003.01700](#)].
- [76] S. Alioli, S. Ferrario Ravasio, J.M. Lindert and R. Röntsch, *Four-lepton production in gluon fusion at NLO matched to parton showers*, *Eur. Phys. J. C* **81** (2021) 687 [[2102.07783](#)].
- [77] B. Agarwal, S.P. Jones and A. von Manteuffel, *Two-loop helicity amplitudes for $gg \rightarrow ZZ$ with full top-quark mass effects*, *JHEP* **05** (2021) 256 [[2011.15113](#)].
- [78] C. Brønnum-Hansen and C.-Y. Wang, *Top quark contribution to two-loop helicity amplitudes for Z boson pair production in gluon fusion*, *JHEP* **05** (2021) 244 [[2101.12095](#)].
- [79] F. Zimmermann, M. Benedikt, M. Capeans Garrido, F. Cerutti, B. Goddard, J. Gutleber et al., *HE-LHC: The High-Energy Large Hadron Collider: Future Circular Collider*

Conceptual Design Report Volume 4. Future Circular Collider, *Eur. Phys. J. ST* **228** (2019) 4.

- [80] M. Benedikt, M. Capeans Garrido, F. Cerutti, B. Goddard, J. Gutleber, J.M. Jimenez et al., *FCC-hh: The Hadron Collider: Future Circular Collider Conceptual Design Report Volume 3. Future Circular Collider*, *Eur. Phys. J. ST* **228** (2019) 4.
- [81] FCC collaboration, *FCC Physics Opportunities: Future Circular Collider Conceptual Design Report Volume 1*, *Eur. Phys. J. C* **79** (2019) 474.
- [82] CMS collaboration, *Prospects for HH measurements at the HL-LHC*, [CMS-PAS-FTR-18-019](#), CERN, Geneva (2018).
- [83] U. Haisch, M. Ruhdorfer, E. Salvioni, E. Venturini and A. Weiler, *Singlet night in Feynman-ville: one-loop matching of a real scalar*, *JHEP* **04** (2020) 164 [[2003.05936](#)].
- [84] D. Gonçalves, T. Han, F. Kling, T. Plehn and M. Takeuchi, *Higgs boson pair production at future hadron colliders: From kinematics to dynamics*, *Phys. Rev. D* **97** (2018) 113004 [[1802.04319](#)].
- [85] W. Bizoń, U. Haisch and L. Rottoli, *Constraints on the quartic Higgs self-coupling from double-Higgs production at future hadron colliders*, *JHEP* **10** (2019) 267 [[1810.04665](#)].
- [86] M. Cepeda et al., *Report from Working Group 2: Higgs Physics at the HL-LHC and HE-LHC*, *CERN Yellow Rep. Monogr.* **7** (2019) 221 [[1902.00134](#)].
- [87] J. de Blas et al., *Higgs Boson Studies at Future Particle Colliders*, *JHEP* **01** (2020) 139 [[1905.03764](#)].
- [88] A. Alloul, N.D. Christensen, C. Degrande, C. Duhr and B. Fuks, *FeynRules 2.0 - A complete toolbox for tree-level phenomenology*, *Comput. Phys. Commun.* **185** (2014) 2250 [[1310.1921](#)].
- [89] T. Hahn, *Generating Feynman diagrams and amplitudes with FeynArts 3*, *Comput. Phys. Commun.* **140** (2001) 418 [[hep-ph/0012260](#)].
- [90] H.H. Patel, *Package-X: A Mathematica package for the analytic calculation of one-loop integrals*, *Comput. Phys. Commun.* **197** (2015) 276 [[1503.01469](#)].